



Contents lists available at ScienceDirect

Journal of Biomechanics

journal homepage: www.elsevier.com/locate/jbiomech
www.JBiomech.com

Effects of local coronary blood flow dynamics on the predictions of a model of in-stent restenosis

Pavel Zun^{a,b,c,*}, Andrey Svitenkov^c, Alfons Hoekstra^b^a Erasmus Medical Center, The Netherlands^b University of Amsterdam, The Netherlands^c ITMO University, Russia

ARTICLE INFO

Article history:

Accepted 22 February 2021

Keywords:

Restenosis model

In silico model

Blood flow model

Boundary conditions

ABSTRACT

Computational models are increasingly used to study cardiovascular disease. However, models of coronary vessel remodelling usually make some strong assumptions about the effects of a local narrowing on the flow through the narrowed vessel. Here, we test the effects of local flow dynamics on the predictions of an in-stent restenosis (ISR) model. A previously developed 2D model of ISR is coupled to a 1D model of coronary blood flow. Then, two different assumptions are tested. The first assumption is that the vasculature is always able to adapt, and the volumetric flow rate through the narrowed vessel is kept constant. The second, alternative, assumption is that the vasculature does not adapt at all, and the ratio of the pressure drop to the flow rate (hydrodynamic resistance) stays the same throughout the whole process for all vessels unaffected by the stenosis, and aortic or venous blood pressure does not change either. Then, the dynamics are compared for different locations in coronary tree for two different reendothelialization scenarios. The assumptions of constant volumetric flow rate (absolute vascular adaptation) versus constant aortic pressure drop and no adaptation do not significantly affect the growth dynamics for most locations in the coronary tree, and the differences can only be observed at the locations where a strong alternative flow pathway is present. On the other hand, the difference between locations is significant, which is consistent with small vessel size being a risk factor for restenosis. These results suggest that the assumption of a constant flow is a good approximation for ISR models dealing with the typical progression of ISR in the most often stented locations such as the proximal parts of left anterior descending (LAD) and left circumflex (LCX) arteries.

© 2021 The Authors. Published by Elsevier Ltd. This is an open access article under the CC BY license (<http://creativecommons.org/licenses/by/4.0/>).

1. Introduction

Coronary artery diseases are a major cause of mortality ([Global Health Estimates 2016: Deaths by Cause, Age, Sex, by Country and by Region, 2000–2016, 2018](#)). Coronary artery narrowing causes ischemia, and makes patients prone to myocardial infarction in case of an acute artery blockage. Artery narrowing is often corrected by performing a percutaneous balloon angioplasty and placing a stent in the affected artery to keep it open. However, in some cases the artery re-narrows due to excessive proliferation of smooth muscle cells (SMCs) in the vessel wall ([Jukema et al., 2012b, 2012a](#)). This proliferation depends on multiple factors, such as presence of intact endothelium in the vessel, extent of arterial injury and also wall shear stress (WSS) inside the artery ([Iqbal et al., 2013b](#)).

WSS is determined by the local flow pattern, which depends on the flow dynamics in the whole coronary arterial tree in addition to the local vessel geometry ([Morlacchi et al., 2011](#)). Coronary vessels adapt to local narrowing and increased hydrodynamic resistance by dilation of the small resistance vessels and by vascular remodelling ([van de Vosse and Stergiopoulos, 2011](#)). These mechanisms can reduce the overall resistance of the arterial pathway and increase the flow to prevent ischemia, but they have their limits and fail for large increases in resistance ([Tuttle et al., 2001](#)).

Models of coronary vessel remodelling, and of restenosis in particular, usually assume one of two extreme cases. The first case is that the vasculature is always able to adapt, and the volumetric flow rate in the narrowed vessel is always kept constant. Physiologically, the assumption of a constant volumetric flow rate means that the perfusion in the tissue downstream of the stenosis is kept at a normal level.

The second extreme is that the vasculature does not adapt at all, and the ratio of the pressure drop to the flow rate (hydrodynamic

* Corresponding author.

E-mail address: p.zun@uva.nl (P. Zun).

resistance) of all vessels unaffected by the stenosis, as well as aortic and venous blood pressure, stay the same throughout the whole process.

In particular, (Caiazzo et al., 2011; Tahir et al., 2013, 2011; Zahedmanesh et al., 2014; Zun et al., 2019, 2017) assume the flow rate is constant in the stented vessel. (Boyle et al., 2013) do not explicitly model the blood flow, but they assume the flow environment to be constant, or that the changes do not affect the neointima formation. (Nolan and Lally, 2018) also do not model the flow, and assume that the local WSS is always high enough to inhibit the growth if intact endothelial cells (ECs) are present. (Escuer et al., 2019) assume a constant pressure inside the stented vessel, while (Keshavarzian et al., 2017) study the homeostasis in the arterial wall under transient increases in blood pressure. An assumption of a constant pressure drop in the stented vessel can be interpreted as a lack of adaptation, where the flow rate through the stenosis drops as its resistance increases.

Both approaches are simplifications of the real process. As the narrowing progresses, the compensatory mechanisms gradually go from alleviating it entirely to becoming more and more inefficient (Werner et al., 2006).

The relation between the stenosis resistance and flow is important because it determines the presence of ischemia in the tissue supported by the affected artery (Taylor et al., 2013). The flow also influences the narrowing dynamics, particularly in case of restenosis. Regions of low WSS, and low flux, are more prone to restenosis, which can result in even higher resistance, lower flux, and lower WSS (Caputo et al., 2013). Low WSS contributes to the development of the initial atherosclerotic lesions as well, by promoting inflammation and leading to a similar feedback loop of outward remodelling, transforming smaller fibroatheromas to high-risk plaques (Chatzizisis et al., 2007; Corti et al., 2020).

Different assumptions about the flow boundary conditions (BCs) lead to potentially different restenosis dynamics. Here we couple our previously developed multiscale agent-based model of in-stent restenosis (ISR) (Tahir et al., 2014) to a 1D model of coronary tree, and test the growth in the resulting model for different BCs.

The authors are not aware of any previous studies coupling a 1D coronary tree model to a model of restenosis progression. Such coupling can result in a reduction of the volumetric flow rate on the stenosis to an even larger extent than simply assigning a constant pressure drop. The reason for this is that if we consider the entire coronary tree, it provides competing flow pathways for blood: parallel vessels with a lower resistance than the stenosed one, which the blood can take to get to the venous system.

We consider two extreme cases described above (absolute vascular adaptation or no vascular adaptation) to determine the extent to which selecting one or the other approximation will affect the progression of restenosis in our model.

The relation between resistance and flux is also affected by the location of a stenosis in the coronary tree and by the individual features of the particular system of coronary arteries. Because of this, here we perform a comparison for stenoses located in different parts of the tree, in both large and small arteries.

2. Materials and methods

We use a fully coupled multiscale two-dimensional model of in-stent restenosis (ISR2D), based on our earlier model, reported in (Tahir et al., 2014) and (Nikishova et al., 2018). It consists of two submodels: an agent-based model of vessel walls, and a lattice Boltzmann model of 2D blood flow. We extend it with a 1D model of a full coronary tree, which is coupled to the 2D model of flow in

the stented segment. The values of flow rate from 1D model are passed to the 2D model as inlet flow.

In the 2D model the detailed flow and the total pressure drop in the stented segment are calculated. From this pressure, the hydrodynamic resistance of the 2D segment is calculated as and passed back to the 1D model, which uses it to update the inlet flow. The 2D flow model also calculates WSS and passes it to the agent-based vessel wall model.

The stochasticity in the model comes from the non-deterministic SMC proliferation rule. The length of each individual cell's cycle is set according to a normal distribution ($\mu = 32$ h, $\sigma = 2$ h). The relative orientation of the daughter cells is chosen randomly during mitosis, and the pattern of reendothelization is random as well.

This model with variable flow through the stenosis is contrasted against a constant flow modification, where the volumetric flow rate in the stented segment of the 1D tree is calculated once at the start of the simulation with an assumption of zero additional resistance in the stented region. In the constant flow scenario, this initial flux value is used throughout the simulation, while for variable flow the flux is recalculated after every iteration of the cell growth model, taking into account the current hydrodynamic resistance of the stented segment.

The stented vessel wall is represented by an agent-based sub-model, which is described in detail in (Tahir et al., 2014). Briefly, this model represents each SMC in the wall as an off-lattice agent. The circle-shaped agents interact with each other through a potential force consisting of elastic repulsion for overlapping agents and linear attraction for non-overlapping neighbouring agents. This model also includes smaller agents on the inner surface of the vessel, which make up the internal elastic lamina (IEL). The endothelium is modelled implicitly, as a probabilistic function of local endothelium function recovery at each time point, assigned to each SMC agent. After stent deployment, the SMCs in the areas wounded by the stent start proliferating, and later stop if any of the following two conditions are fulfilled. One: the local endothelium has recovered, and the local WSS is high enough for the ECs to produce enough nitric oxide (NO) to suppress SMC growth. Two: the SMC in question is deep in the vessel wall, has no space to grow, and is contact inhibited (in the model it translates to a high number of neighbouring cells).

Uninhibited SMCs perform a cell growth cycle, during which they grow to twice their initial size, and then undergo mitosis and split into two daughter cells.

These agents make up a longitudinal section of an artery, composed of two arterial walls (Fig. 1). The stent is represented as square struts which are pressed into the vessel wall, deforming and damaging it, rupturing the IEL and destroying SMCs. In addition to the damage caused by the struts, the endothelium at the site of stenting is assumed to be completely denuded by the balloon inflation during angioplasty. After deployment, proliferation

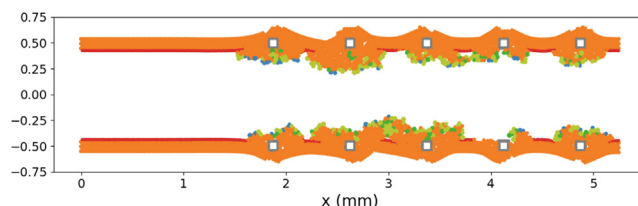


Fig. 1. Example computational domain used in one of the simulations reported in this paper (location #1), 300 h after stenting. This geometry includes an inlet region (flow from left to right) and five pairs of struts. Orange circles are individual SMCs, red circles are IEL agents, and grey circles make up the stent struts. Green cells are synthetic and proliferating, blue are nitric oxide (NO) inhibited. Proliferating SMCs can be seen in the lumen. (For interpretation of the references to colour in this figure legend, the reader is referred to the web version of this article.)

starts from the damaged locations (Fig. 1). For the simulations carried out in this paper, a region with several stent struts was considered, and an unstented inlet segment was added to the region to allow the flow to develop. Two different scenarios for reendothelialization were considered, similar to those used in our previous publications (Nikishova et al., 2018; Tahir et al., 2014): one where 59% of endothelium recovers during the first three days, and the rest recovers fully after 23 days (normal reendothelialization scenario), and a second where the initial fast recovery is absent, and the endothelium recovers linearly over 23 days (slow reendothelialization scenario). We include both of these scenarios because the model is sensitive to the reendothelialization speed (slower recovery means larger growth) (Nikishova et al., 2018), and may interact with the flow differently if there is already a significant restenosis by the time the endothelium recovers.

The 1D model of coronary blood flow represents the flow in large coronary vessels. It is similar to the model described in (Alastruey et al., 2011), and is based on the implementation by (Svitenkov et al., 2018). However, in (Svitenkov et al., 2018) the model is extended with propagation of contrast agent through arteries, while here only the flow of blood is considered. Briefly, the 1D model describes a pulsatile blood flow through elastic cylindrical vessels, with special conditions for bifurcations, and the stenosis is modelled as a hydrodynamic resistance element. Smaller vessels are abstracted as Windkessel BCs. By adjusting BCs, the model is calibrated to provide a flux similar to the normal resting flux in humans. The model is applied to the human left coronary tree geometry (Fig. 2).

The coupling between the agent-based model and the 2D flow model has been described in detail in (Nikishova et al., 2018). The mapping of WSS for each cell is done by looping over all lattice nodes in the vicinity. If the cell overlaps with a circle circumscribed around the (square) lattice node, the node is counted towards the average WSS. The lattice nodes in the solid wall, which have zero shear stress, are ignored in this procedure, and WSS values only come from liquid nodes. The average is calculated as an arithmetic mean of the non-zero shear stress values. Mesh generation for the 2D flow solver from cell positions is done similarly: if a node intersects with a cell, it is marked as a part of the solid wall, and if there are no intersections, liquid can flow through it.

The coupling between the 1D and 2D flow models is done by passing the inlet flow rate from 1D to 2D on every iteration of the agent-based model, and by passing the hydrodynamic resistance back from 2D to 1D. For each resistance value, the 1D model is executed for several heart cycles to let the flow stabilize. Our

assumption is that NO production by the endothelium is governed by the time-averaged WSS (TAWSS), so the 2D flow model operates under an assumption of a steady flow. To make a steady flow profile, the flow rate calculated by the 1D model is averaged over the cardiac cycle, and the result is passed to the 2D model.

The flux from 1D model assumes cylindrical vessels, while the agent-based wall model simulates the proliferation on two opposite parallel walls, which does not directly transform into growth in a cylindrical vessel (Zun et al., 2017). Because of this, some transformations are required to convert the data from the 1D model to a 2D parallel plate flow. Based on the flux of a 3D Poiseuille flow (Sutera and Skalak, 1993), a 2D flow with the same maximum velocity is generated:

$$Q_{cyl} = \frac{\pi r^4 (p_1 - p_2)}{8\eta L} = \frac{\pi r^2 v_{max}}{2} \quad (1)$$

$$v_{max} = \frac{2Q_{cyl}}{\pi r^2} = \frac{(p_1 - p_2)r^2}{4\eta L} \quad (2)$$

where Q_{cyl} is the flow for a cylindrical vessel of radius r , p_1 and p_2 are the inlet and outlet pressures, η is the viscosity, L is the length of the vessel, and v_{max} the maximum velocity of the liquid. The two-plate flow is then prescribed as parabolic, with zero velocity at the wall-lumen border and v_{max} at the lumen centre.

Hydrodynamic resistance R is defined as the ratio of the pressure drop to the flow rate. To calculate the expected pressure drop for a 3D segment, we use Q_{cyl} and the inlet and outlet pressures p_{in} and p_{out} from the 2D simulation:

$$R = \frac{p_{in} - p_{out}}{Q_{cyl}} \quad (3)$$

This resistance is then passed back to the 1D model. Since in our 2D model we do not consider the entire stent, but only a few of its struts (specifically, five struts evenly spaced over a 3 mm long vessel segment), the resistance, which is linearly proportionate to the vessel length for cylindrical vessels, is then scaled $10 \times$ to calculate the resistance of a full-size stent (Iqbal et al., 2013a).

To assess the vessel patency, relative lumen loss was calculated for the stented regions for every time step of the agent-based model. To do that, vessel radius was measured for all points between the 1st and the last stent struts, then lumen area was calculated for these points assuming a circular lumen, and the resulting areas were averaged over the stented segment.

Since the vessel's size and its environment are likely to affect the dynamics of blood flow and restenosis, multiple locations in both LAD (locations #5, #7), LCX (#2), and their branches (#1, #3, #4, #6, #8) were used to test our hypothesis (see Fig. 2). For each of the locations, constant and variable flow conditions were considered, as described above. In each of the considered scenarios, for each of these cases, the model was executed ten times to account for the stochasticity, and to obtain the average growth and the standard deviations. The number of simulations was chosen based on the uncertainty quantification performed in (Nikishova et al., 2018).

3. Results

3.1. Static and dynamic flow approximation for 1D model

For this series of simulations, the reendothelialization scenario with fast recovery before the 3rd day was used, as described above. For these cases, the resistance value for each time step was calculated according to formula (3). By comparing the resistance differences, we see that for most of the considered locations the resistance values are extremely close for the two flow assumptions

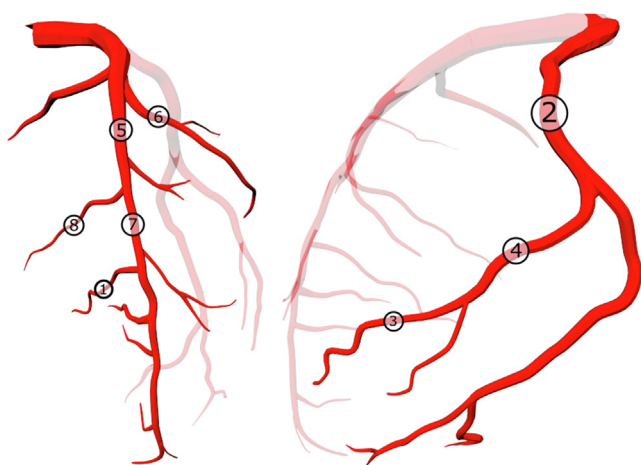


Fig. 2. 3D model of the geometry used in the 1D flow model, two projections. Highlighted arteries, left: LAD and its branches; right: LCX and its branches. The locations of stents considered in this paper are marked by numbers.

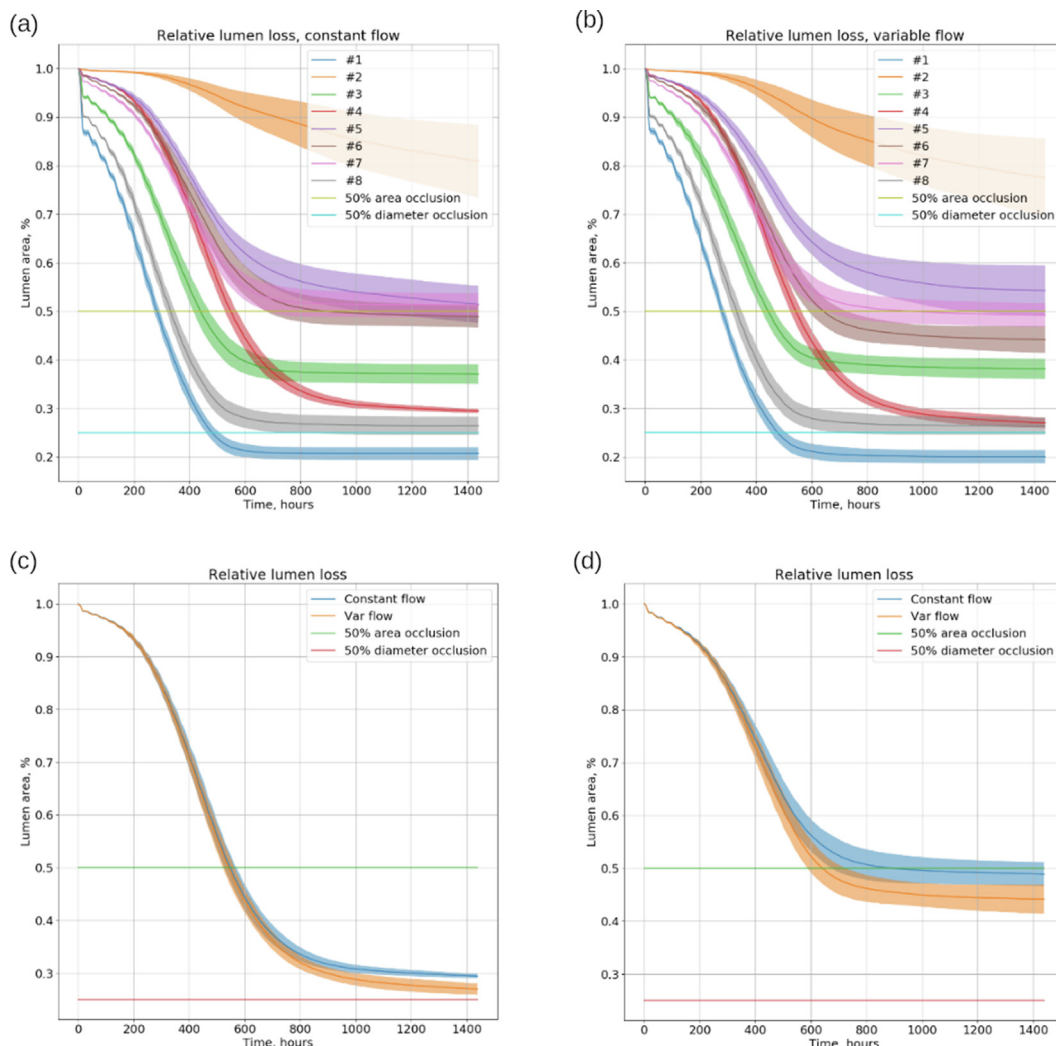


Fig. 3. Relative lumen area loss dynamics for assumptions of constant and variable flow for different locations in the coronary tree; (a) general plot for constant flow, (b) general plot for variable flow, (c) and (d) detailed plots for the two locations (#4 and #6 respectively) where there are noticeable differences in the endpoint lumen area between the two assumptions. Horizontal lines denote 50% area and 50% diameter occlusion. Shaded regions show the standard error for each location.

considered. Fig. 3 (a) and (b) show the lumen area loss inside the stent for assumption of constant (a) and variable (b) flux in the stented vessel. For all locations except #4 and #6 these resistance values are within one standard deviation from each other for the endpoint, and for #4 and #6 they are within three standard deviations of each other. The latter two locations are in side branches with a strong competing flow pathway (see Fig. 2). Fig. 3 (c), (d) show the lumen loss dynamics in these locations in more detail.

Table 1
Final average SMC counts in the normal reendothelization scenario, for the constant and variable flow cases.

Site #	Final SMC count, constant flow case	Final SMC count, variable flow case
1	4278	4273
2	4476	4276
3	5470	5626
4	8156	8545
5	4238	4257
6	4437	4433
7	4152	4253
8	4715	4880

The quantity of tissue being made is different for different vessels; e.g. at sites #2 and #4 the proliferation goes on for a long time, while at sites #1, #3, and #8 it stops early, which can be seen in the plot. Starting from the initial 2000 SMCs, most locations proliferate to between 3506 and 6103 cells (averages for each location presented in Table 1), with the exception of location #4, which at the endpoint has 8156 cells on average for the constant flow scenario, and 8545 cells on average for the variable flow scenario.

3.2. Location in the coronary tree

Fig. 3 also shows that while for most locations the assumption of constant versus variable flow does not have much of an effect, the location in the coronary tree matters a lot for the progression of restenosis.

The area loss varies from 18% to 80%, and the corresponding flux reduction for variable flow scenario at simulation endpoint varies from 2% (location #2, proximal third of LCX) to 40% (location #1, small side branch originating from LAD).

This is consistent with the fact that small vessel size (less than 3.0 mm diameter) is considered an independent risk factor for the occurrence of ISR (Briguori et al., 2002).

3.3. Slow endothelial recovery

For the series of simulations described below, slow reendothelization scenario was used in order to exaggerate the restenosis and its effects on impeding the flow through the stented arteries. This slow reendothelization scenario represents the case when the endothelial recovery is disrupted in the patient for some reason. We do not investigate specific reasons for this, and instead use this case to see if this delayed reendothelization would amplify the feedback loop between the flow reduction and the growth.

For site #1, all simulations predicted lumen width less than 0.015 mm (lattice size of the flow solver) at some point between three and four weeks after stenting, essentially leading to a total coronary occlusion. Because of this, the simulations could not proceed to the 60 days endpoint, and site #1 was excluded from analysis.

In other locations, also more growth was seen than in the previous scenario (Fig. 4 (a), (b)). However, similarly to the previous scenario, only locations #4 and #6 show differences above one standard deviation in the end lumen area (Fig. 4 (c), (d)).

4. Discussion

The main finding of this study is that the two assumptions, for the specific scenario of restenosis modelling, have little impact on the predicted growth. There is not much impact on the growth prediction if we choose to fully couple the 1D model of the coronary tree to the growth model, as opposed to using the initial flow rate measurement to set the boundary conditions. There are however exceptions to this, highlighted in the panels (c) and (d) in Figs. 3 and 4, which have to be taken into the account for those or similar locations. Especially the location #6 in the proximal part of the left marginal artery may be of interest for clinicians, since in some patients this artery is a major supplier of blood for the left ventricle.

For the field of restenosis modelling this means that for most cases it is sufficient to use the constant flow assumption, which is easier to realise, since it does not require the knowledge of the whole coronary tree and is also computationally cheaper. This is also very relevant for any potential personalized applications of restenosis models, since our findings show it is sufficient to know the local flow properties to sufficiently inform the flow model. These local properties may be, for example, an optical coherence

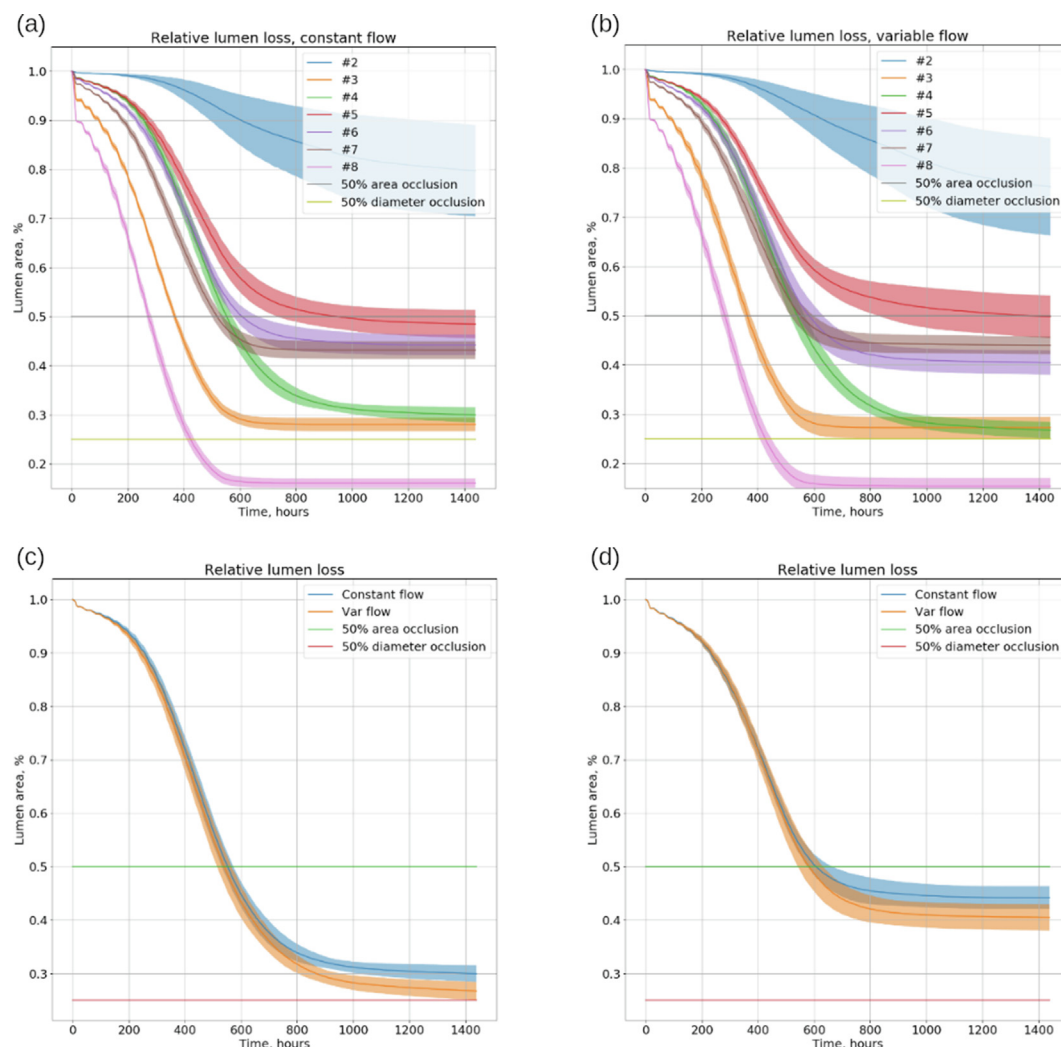


Fig. 4. Relative lumen area loss dynamics for assumptions of constant and variable flow for different locations in the coronary tree, slow initial endothelium recovery; (a) general plot for constant flow, (b) general plot for variable flow, (c) and (d) detailed plots for the two locations (#4 and #6 respectively) where there are noticeable differences in the endpoint lumen area between the two assumptions. Horizontal lines denote 50% area and 50% diameter occlusion. Shaded regions show the standard error for each location.

tomography (OCT) scan of the affected vessel segment together with a Doppler measurement of the local blood velocity. These measurements could be obtained during the coronary intervention. Reconstructing the entire coronary tree, even as a 1D network, would add a significant challenge. Reconstruction from multiple angiography images would also introduce large uncertainties, since the blood vessel borders are diffuse in the images, meaning we cannot know their radius exactly, and smaller vessels, which contribute much in terms of hydraulic resistance, are not visible at all.

However, this is only true when we only consider the extent of growth, and not the impact on the flow. For estimation of (virtual) fractional flow reserve (FFR) (Carson et al., 2019) it may be necessary to consider more detailed boundary conditions.

The total flow can be greatly reduced, which together with the differences in pressure drop can lead to significant variations in vFFR. The importance of boundary conditions for vFFR estimation has been demonstrated earlier, e.g. in (Boileau and Nithiarasu, 2015) and in (Gamilov et al., 2015).

The model of ISR considered in this publication is a very simple one. More detailed and advanced models exist (Zun et al., 2019), however they are much more computationally expensive due to modelling a larger 3D domain. They give better predictions of ISR progression, however ultimately the qualitative relation between the WSS and the growth is similar. Because of this, we can assume that the conclusions about the effects of flow BCs drawn from this simple 2D model will also hold for more advanced models.

In addition to being 2D, the model of ISR considered in this paper also makes several important assumptions that affect the final resistance of the vessel. First of all, the vessel is assumed to be straight, while coronary vessels *in vivo* have a significant curvature, which increases the resistance. Second, the model ignores a lot of the finer details of neointimal formation. One big omission is the extracellular matrix (ECM) formation. The studies find that more than 50% of the neointimal volume is made up of ECM, while the model assumes that the neointima consists purely of SMCs. The lack of ECM causes the neointimal volume, and the resulting resistance, to be underestimated.

In addition, the model ignores the early processes happening after stenting, such as inflammation and thrombus formation. Instead, the model assumes that neointima formation by SMC proliferation starts immediately after stenting and that SMC proliferation dominates the process. However, there is evidence that there is little SMC proliferation early on, and the vessel is covered in a thin thrombus (Grewe et al., 2000; Malik et al., 1998). These processes might delay the neointima formation, resulting in a smaller overall growth.

Another issue is that, while most of the model parameters in the considered scenarios are based on human data, the endothelium regeneration time is based on porcine results used in a previous publication (Tahir et al., 2014), since the endothelium regeneration data for humans is not readily available. The porcine data was produced by euthanising the animals and performing tissue histometry (Van Beusekom et al., 2012), and the related human data is scarce, based on autopsy reports (Grewe et al., 2000), and further confounded by the fact that the considered vessels are diseased and in some cases stent failure is the very reason of death. However, similarly to the difference between the 2D model used here and the more complicated 3D models, this discrepancy should not affect the main conclusions of this paper, since the overall mechanisms involved in the porcine and in the human restenosis are similar, and the main difference lies in the time course of this process (Iqbal et al., 2016): in porcine arteries the process takes about four weeks, and in human arteries remodelling can take up to six months (Schwartz et al., 1996).

5. Conclusions

In this paper a study of the effects of flow boundary conditions and the location in coronary tree on a previously developed two-dimensional model of ISR (Tahir et al., 2014) are presented. This model has been coupled to a one-dimensional model of pulsatile coronary blood flow, also previously developed, which is used to provide time-averaged flux to the neointimal growth model.

The simulation results suggest that the assumptions of constant flow (absolute vascular adaptation) versus constant aortic pressure drop and no adaptation do not significantly affect the growth dynamics for most locations in the coronary tree, and the differences can only be observed at the locations where a strong alternative flow pathway is present.

On the other hand, the difference between locations is significant, which is consistent with small vessel size being a risk factor for restenosis. These results also suggest that assumption of constant flow is a good approximation for ISR models dealing with the typical progression of ISR in the most often stented locations such as the proximal parts of LAD and LCX.

Acknowledgements

The authors thank Lourens Veen (Netherlands eScience Center) for his help with developing the software for ISR simulations and for setting up the simulation runs on HPC architecture.

PZ and AS acknowledge partial funding from the Russian Foundation for Basic Research under agreement #18-015-00504; AS acknowledges partial funding from The Russian Science Foundation under agreement #20-71-10108; PZ acknowledges partial funding from the EU Horizon 2020 programme under Grant Agreement 777119, the InSilc project. This work is supported by the Netherlands eScience Center and NWO under the e-MUSC project.

References

- Alastruey, J., Khir, A.W., Matthys, K.S., Segers, P., Sherwin, S.J., Verdonck, P.R., Parker, K.H., Peiró, J., 2011. Pulse wave propagation in a model human arterial network: Assessment of 1-D visco-elastic simulations against *in vitro* measurements. *J. Biomech.* 44, 2250–2258. <https://doi.org/10.1016/j.jbiomech.2011.05.041>.
- Boileau, E., Nithiarasu, P., 2015. One-Dimensional Modelling of the Coronary Circulation. Application to Noninvasive Quantification of Fractional Flow Reserve (FFR). in: Tavares J., Natal Jorge R. (Eds) Computational and Experimental Biomedical Sciences: Methods and Applications. Lecture Notes in Computational Vision and Biomechanics, Vol 21. pp. 137–155. https://doi.org/10.1007/978-3-319-15799-3_11.
- Boyle, C.J., Lennon, A.B., Prendergast, P.J., 2013. Application of a mechanobiological simulation technique to stents used clinically. *J. Biomech.* 46, 918–924. <https://doi.org/10.1016/j.jbiomech.2012.12.014>.
- Briguori, C., Sarais, C., Pagnotta, P., Liistro, F., Montorfano, M., Chieffo, A., Sgura, F., Corvaja, N., Albiero, R., Stankovic, G., Toutoutzas, C., Bonizzoni, E., Di Mario, C., Colombo, A., 2002. In-stent restenosis in small coronary arteries. *J. Am. Coll. Cardiol.* 40, 403–409. [https://doi.org/10.1016/S0735-1097\(02\)01989-7](https://doi.org/10.1016/S0735-1097(02)01989-7).
- Caiazzo, A., Evans, D., Falcone, J.L., Hegewald, J., Lorenz, E., Stahl, B., Wang, D., Bernsdorf, J., Chopard, B., Gunn, J.P., Hose, D.R., Krafczyk, M., Lawford, P.V., Smallwood, R., Walker, D., Hoekstra, A.G., 2011. A Complex Automata approach for in-stent restenosis: Two-dimensional multiscale modelling and simulations. *J. Comput. Sci.* 2, 9–17. <https://doi.org/10.1016/j.jocs.2010.09.002>.
- Caputo, M., Chiastra, C., Cianciolo, C., Cutri, E., Dubini, G., Gunn, J., Keller, B., Migliavacca, F., Zunino, P., 2013. Simulation of oxygen transfer in stented arteries and correlation with in-stent restenosis. *Int. J. Numer. Method. Biomed. Eng.* 29, 1373–1387. <https://doi.org/10.1002/cnm.2588>.
- Carson, J., Pant, S., Roobottom, C., Alcock, R., Blanco, P.J., Bulant, C.A., Vassilevski, Y., Simakov, S., Gamilov, T., Pryamonosov, R., Liang, F., Ge, X., Liu, Y., Nithiarasu, P., 2019. Non-invasive coronary CT angiography-derived fractional flow reserve (FFR): A benchmark study comparing the diagnostic performance of four different computational methodologies. *Int. J. Numer. Method. Biomed. Eng.* 1–22. <https://doi.org/10.1002/cnm.3235>.
- Chatzizisis, Y.S., Coskun, A.U., Jonas, M., Edelman, E.R., Stone, P.H., Feldman, C.L., 2007. Risk stratification of individual coronary lesions using local endothelial shear stress: a new paradigm for managing coronary artery disease. *Curr. Opin. Cardiol.* 22, 552–564. <https://doi.org/10.1097/HCO.0b013e3282f07548>.

- Corti, A., Chiastra, C., Colombo, M., Garbey, M., Migliavacca, F., Casarin, S., 2020. A fully coupled computational fluid dynamics – agent-based model of atherosclerotic plaque development: Multiscale modeling framework and parameter sensitivity analysis. *Comput. Biol. Med.* 118. <https://doi.org/10.1016/j.combiomed.2020.103623>. 103623.
- Escuer, J., Martinez, M., McGinty, S., Pena, E., 2019. Mathematical modelling of the restenosis process after stent implantation. *J. R. Soc. Interface*.
- Gamilov, T.M., Kopylov, P.Y., Pryamonosov, R.A., Simakov, S.S., 2015. Virtual fractional flow reserve assessment in patient-specific coronary networks by 1D hemodynamic model. *Russ. J. Numer. Anal. Math. Model.* 30, 269–276. <https://doi.org/10.1515/rnam-2015-0024>.
- Global Health Estimates, 2016. Deaths by Cause, Age, Sex, by Country and by Region, 2000–2016, 2018. World Health Organization, Geneva.
- Grewe, P.H., Deneke, T., Machraoui, A., Barmeyer, J., Müller, K.-M., 2000. Acute and Chronic Tissue Response to Coronary Stent Implantation: Pathologic Findings in Human Specimen. [https://doi.org/10.1016/S0735-1097\(99\)00486-6](https://doi.org/10.1016/S0735-1097(99)00486-6).
- Iqbal, J., Chamberlain, J., Francis, S.E., Gunn, J., 2016. Role of Animal Models in Coronary Stenting. *Ann. Biomed. Eng.* 44, 453–465. <https://doi.org/10.1007/s10439-015-1414-4>.
- Iqbal, J., Gunn, J.P., Serruys, P.W., 2013a. Coronary stents: historical development, current status and future directions. *Br. Med. Bull.* 106, 193–211. <https://doi.org/10.1093/bmb/ldt009>.
- Iqbal, J., Serruys, P.W., Taggart, D.P., 2013b. Optimal revascularization for complex coronary artery disease. *Nat. Rev. Cardiol.* 10, 635–647. <https://doi.org/10.1038/nrcardio.2013.138>.
- Jukema, J.W., Ahmed, T.A.N., Verschuren, J.J.W., Quax, P.H.A., 2012a. Restenosis after PCI. Part 2: prevention and therapy. *Nat. Rev. Cardiol.* 9, 79–90. <https://doi.org/10.1038/nrcardio.2011.148>.
- Jukema, J.W., Verschuren, J.J.W., Ahmed, T.A.N., Quax, P.H.A., 2012b. Restenosis after PCI. Part 1: pathophysiology and risk factors. *Nat. Rev. Cardiol.* 9, 53–62. <https://doi.org/10.1038/nrcardio.2011.132>.
- Keshavarzian, M., Meyer, C.A., Hayenga, H.N., 2017. Mechanobiological model of arterial growth and remodeling. *Biomech. Model. Mechanobiol.* 17, 1–15. <https://doi.org/10.1007/s10237-017-0946-y>.
- Malik, N., Gunn, J.P., Holt, C.M., Shepherd, L., Francis, S.E., Newman, C.M.H., Crossman, D.C., Cumberland, D.C., 1998. Intravascular stents: a new technique for tissue processing for histology, immunohistochemistry, and transmission electron microscopy. *Heart* 80, 509–516. <https://doi.org/10.1136/hrt.80.5.509>.
- Morlacchi, S., Keller, B.K., Arcangeli, P., Balzan, M., Migliavacca, F., Dubini, G., Gunn, J.P., Arnold, N., Narracott, A.J., Evans, D., Lawford, P., 2011. Hemodynamics and In-stent restenosis: Micro-CT images, histology, and computer simulations. *Ann. Biomed. Eng.* 39, 2615–2626. <https://doi.org/10.1007/s10439-011-0355-9>.
- Nikishova, A., Veen, L., Zun, P., Hoekstra, A.G., 2018. Uncertainty Quantification of a Multiscale Model for In-Stent Restenosis. *Cardiovasc. Eng. Technol.* 9, 761–774. <https://doi.org/10.1007/s13239-018-00372-4>.
- Nolan, D.R., Lally, C., 2018. An investigation of damage mechanisms in mechanobiological models of in-stent restenosis. *J. Comput. Sci.* 24, 132–142. <https://doi.org/10.1016/j.jocs.2017.04.009>.
- Schwartz, R.S., Chu, A., Edwards, W.D., Srivatsa, S.S., Simari, R.D., Isner, J.M., Holmes, D.R., 1996. A proliferation analysis of arterial neointimal hyperplasia: Lessons for antiproliferative restenosis therapies. *Int. J. Cardiol.* 53, 71–80. [https://doi.org/10.1016/0167-5273\(95\)02499-9](https://doi.org/10.1016/0167-5273(95)02499-9).
- Sutera, S.P., Skalak, R., 1993. The History of Poiseuille's Law. *Annu. Rev. Fluid Mech.* 25, 1–20.
- Svitenkov, A., Pavlov, I., Chivilikhin, S.A., 2018. A one-dimensional model of agent propagation in arterial blood flow. *Procedia Comput. Sci.* 136, 416–424. <https://doi.org/10.1016/j.procs.2018.08.272>.
- Tahir, H., Bona-Casas, C., Hoekstra, A.G., 2013. Modelling the effect of a functional endothelium on the development of in-stent restenosis. *PLoS ONE* 8, e66138. <https://doi.org/10.1371/journal.pone.0066138>.
- Tahir, H., Bona-Casas, C., Narracott, A.J., Iqbal, J., Gunn, J.P., Lawford, P.V., Hoekstra, A.G., 2014. Endothelial repair process and its relevance to longitudinal neointimal tissue patterns: comparing histology with in silico modelling. *J. R. Soc. Interface* 11, 20140022. <https://doi.org/10.1098/rsif.2014.0022>.
- Tahir, H., Hoekstra, A.G., Lorenz, E., Lawford, P.V., Hose, D.R., Gunn, J.P., Evans, D.J.W., 2011. Multi-scale simulations of the dynamics of in-stent restenosis: impact of stent deployment and design. *Interface Focus* 1, 365–373. <https://doi.org/10.1098/rsfs.2010.0024>.
- Taylor, C.A., Fonte, T.A., Min, J.K., 2013. Computational fluid dynamics applied to cardiac computed tomography for noninvasive quantification of fractional flow reserve: Scientific basis. *J. Am. Coll. Cardiol.* 61, 2233–2241. <https://doi.org/10.1016/j.jacc.2012.11.083>.
- Tuttle, J.L., Nachreiner, R.D., Bhuller, A.S., Condict, K.W., Connors, B.A., Herring, B.P., Dalsing, M.C., Unthank, J.L., 2001. Shear level influences resistance artery remodeling: wall dimensions, cell density, and eNOS expression. *Am. J. Physiol. Heart Circ. Physiol.* 281, H1380–H1389.
- Van Beusekom, H.M.M., Ertaş, G., Sorop, O., Serruys, P.W., Van Der Giessen, W.J., 2012. The Genous™ endothelial progenitor cell capture stent accelerates stent re-endothelialization but does not affect intimal hyperplasia in porcine coronary arteries. *Catheter. Cardiovasc. Interv.* 79, 231–242. <https://doi.org/10.1002/ccd.22928>.
- van de Vosse, F.N., Stergiopoulos, N., 2011. Pulse Wave Propagation in the Arterial Tree. *Annu. Rev. Fluid Mech.* 43, 467–499. <https://doi.org/10.1146/annurev-fluid-122109-160730>.
- Werner, G.S., Fritzenwanger, M., Prochnau, D., Schwarz, G., Ferrari, M., Aarnoudse, W., Pijls, N.H.J., Figulla, H.R., 2006. Determinants of Coronary Steal in Chronic Total Coronary Occlusions. Donor Artery, Collateral, and Microvascular Resistance. *J. Am. Coll. Cardiol.* 48, 51–58. <https://doi.org/10.1016/j.jacc.2005.11.093>.
- Zahedmanesh, H., Van Oosterwyck, H., Lally, C., 2014. A multi-scale mechanobiological model of in-stent restenosis: deciphering the role of matrix metalloproteinase and extracellular matrix changes. *Comput. Methods Biomech. Biomed. Engin.* <https://doi.org/10.1080/10255842.2012.716830>.
- Zun, P.S., Anikina, T., Svitenkov, A., Hoekstra, A.G., 2017. A comparison of fully-coupled 3D in-stent restenosis simulations to In-vivo Data. *Front. Physiol.* 8, 284. <https://doi.org/10.3389/fphys.2017.00284>.
- Zun, P.S., Narracott, A.J., Chiastra, C., Gunn, J., Hoekstra, A.G., 2019. Location-Specific Comparison Between a 3D In-Stent Restenosis Model and Micro-CT and Histology Data from Porcine In Vivo Experiments. *Cardiovasc. Eng. Technol.* 10, 568–582. <https://doi.org/10.1007/s13239-019-00431-4>.